Mechanism of Calmodulin Recognition of the Binding Domain of Isoform 1b of the Plasma Membrane Ca^{2+}-ATPase: Kinetic Pathway and Effects of Methionine Oxidation†

Brian D. Slaughter,‡ Ramona J. Bieber Urbauer,§ Jeffrey L. Urbauer,§ and Carey K. Johnson*,‡

Department of Chemistry, 1251 Wescoe Hall Drive, University of Kansas, Lawrence, Kansas 66045-7582, and Department of Chemistry and Department of Biochemistry and Molecular Biology, University of Georgia, Athens, Georgia 30602

Received December 1, 2006; Revised Manuscript Received February 1, 2007

ABSTRACT: Calmodulin (CaM) binds to a domain near the C-terminus of the plasma membrane Ca^{2+}-ATPase (PMCA), causing the release of this domain and relief of its autoinhibitory function. We investigated the kinetics of dissociation and binding of Ca^{2+}-CaM with a 28-residue peptide [C28W(1b)] corresponding to the CaM-binding domain of isoform 1b of PMCA. CaM was labeled with a fluorescent probe on either the N-terminal domain at residue 34 or the C-terminal domain at residue 110. Formation of complexes of CaM with C28W(1b) results in a decrease in the fluorescence yield of the fluorophore, allowing the kinetics of dissociation or binding to be detected. Using a maximum entropy method, we determined the minimum number and magnitudes of rate constants required to fit the data. Comparison of the fluorescence changes for CaM labeled on the C-terminal or N-terminal domain suggests sequential and ordered binding of the C-terminal and N-terminal domains of CaM with C28W(1b). For dissociation of C28W(1b) from CaM labeled on the N-terminal domain, we observed three time constants, indicating the presence of two intermediate states in the dissociation pathway. However, for CaM labeled on the C-terminal domain, we observed only two time constants, suggesting that the fluorescence label on the C-terminal domain was not sensitive to one of the kinetic steps. The results were modeled by a kinetic mechanism in which an initial complex forms upon binding of the C-terminal domain of CaM to C28W(1b), followed by binding of the N-terminal domain, and then formation of a tight binding complex. Oxidation of methionine residues in CaM resulted in significant perturbations to the binding kinetics. The rate of formation of a tight binding complex was reduced, consistent with the poorer effectiveness of oxidized CaM in activating the Ca^{2+} pump.

Calmodulin is a cellular Ca^{2+} sensor that interacts with numerous target enzymes in response to changes in intracellular Ca^{2+} concentrations. The geometries of complexes between CaM[1] and target domains are diverse, as CaM and the target may form not only compact structures but also more extended bound conformations (*1*). It is well-established that the C-terminal domain of CaM binds Ca^{2+} with an ∼1 order of magnitude higher affinity than the N-terminal domain (*2*, *3*), and it also binds more tightly than the N-terminal domain to some targets (*4*, *5*).

One important CaM target is the plasma membrane Ca^{2+}-ATPase (PMCA), a membrane Ca^{2+} pump critical for regulation of intracellular Ca^{2+} levels (*6*, *7*). Several researchers have speculated that an intermediate in the CaM-mediated activation of PMCA corresponds to a bound C-domain of CaM but a free N-domain (*4*, *5*, *8*). However, despite being a potentially crucial link in the model of CaM activation of PMCA, it is still uncertain whether this intermediate exists and, if it does, what rate constants govern its appearance and disappearance. A solution structure of CaM bound to C20W, a 20-residue segment of the CaM-binding domain of PMCA isoform 4b, shows the C-terminal domain of CaM bound to the peptide while the N-terminal domain is free [PDB entry 1cff (*4*)]. Other experiments show that a peptide with just four more residues (C24W) binds in a final structure where both terminal domains of CaM interact with the target (*9*, *10*). Squier and co-workers (*5*) showed that CaM_C (residues 74−144 of CaM) can activate PMCA, but only upon addition of a sufficiently high concentration of CaM_C to allow for two CaM_C molecules to bind to each activated PMCA. Whereas CaM_N (residues 1−74) is also able to fully activate PMCA, a much higher concentration is needed. These results suggest that although the C-terminal

† This research was supported by NIH Grant R01 GM58715. B.D.S. acknowledges support from the Dynamic Aspects of Chemical Biology NIH training grant (NIH 5 T32 GM08545-09).

* To whom correspondence should be addressed. E-mail: ckjohnson@ku.edu. Telephone: (785) 864-4219. Fax: (785) 864-5396.

‡ University of Kansas.

§ University of Georgia.

[1] Abbreviations: C28W(1b), 28-residue CaM-binding domain from isoform 1b of the plasma membrane Ca^{2+}-ATPase; CaM, calmodulin; CaM_{ox}, oxidized calmodulin; EGTA, ethylene glycol bis(2-aminoethyl ether)-*N*,*N*,*N*′,*N*′-tetraacetic acid; HEPES, *N*-(2-hydroxyethyl)piperazine-*N*′-(4-butanesulfonic acid); PMCA, plasma membrane Ca^{2+}-ATPase; T34C-CaM-AF488, calmodulin T34C mutant fluorescently labeled at Cys34 with Alexa Fluor 488; T110C-CaM-AF488, calmodulin T110C mutant fluorescently labeled at Cys110 with Alexa Fluor 488.

10.1021/bi602481u CCC: $37.00
Published on Web 03/08/2007

domain of CaM may interact more tightly with PMCA, two domains must interact simultaneously with PMCA to fully activate the enzyme.

Despite being the isoform expressed in the most tissues (*11*), isoform 1 has been rarely studied due to difficulties in expression (*12*, *13*). Recent studies have examined the kinetics of the interaction of CaM with isoform 4b of PMCA (*14*, *15*). In our study, kinetic measurements are reported for the complex of CaM with the 28-residue CaM-binding domain of PMCA isoform 1b [denoted C28W(1b)]. By comparison of the response for CaM fluorescently labeled in the C-terminal or N-terminal domain, it was possible to determine the order of binding of the C- and N-terminal domains. The goal was to determine the kinetics of C28W(1b) binding at high Ca^{2+} concentrations. However, experimentally, it is useful to probe both the forward and reserve (dissociation) reactions, which are, of course, governed by the same set of time constants. Interaction of CaM with C28W(1b) was detected by fluorescence quenching of the probe Alexa Fluor 488 (AF488) tethered to CaM via cysteine residues introduced into CaM at either position 34 or 110. The rate of fluorescence change upon binding or dissociation of C28W(1b) by CaM was monitored and compared to kinetic models to obtain information about the kinetics of binding and the existence and nature of intermediate structures. For the complex of CaM with C28W(1b), the dissociation process was best characterized by multiple time constants, demonstrating a dissociation mechanism that includes intermediate species. Slow isomerization steps were also observed, which are likely associated with initial steps in the dissociation of the high-affinity CaM−C28W(1b) complex. An additional rate constant was required to fit the data for CaM labeled at the N-terminal domain relative to the CaM labeled at the C-terminal domain, evidence of an intermediate in the pathway that involves changes experienced uniquely by the N-terminal domain of CaM.

We also investigated the effect of oxidation of methionine residues in CaM on its dissociation from C28W(1b). Methionine residues comprise a large component of the binding clefts of CaM (*16*). Oxidation of methionine residues to the sulfoxides in CaM, specifically of methionine residues near the C-terminus, is known to greatly decrease the potency of CaM to activate PMCA (*17*−*19*). This result has important implications for oxidative stress, calcium homeostasis, and aging (*18*, *20*). In addition, oxidation of CaM alters its association with the CaM-binding domain of PMCA (*21*). Thus, using fluorescently labeled oxidized CaM molecules, we investigated the effects of CaM oxidation on the kinetics of dissociation of CaM from C28W(1b) to examine mechanistically how oxidation affects recognition by the PMCA. The observed changes after oxidation suggest a reduced propensity for oxidized CaM to form the tightly binding conformations that may be necessary for full activation of the enzyme.

EXPERIMENTAL PROCEDURES

Materials. Escherichia coli strain BL21(DE3) and the pET-15b expression vector were purchased from Novagen (Madison, WI). All other restriction and modifying enzymes, reagents, and cells were purchased from Invitrogen (Carlsbad, CA). Phenyl Sepharose CL-4B resin and Sephedex-G25 (fine grade) were purchased from Amersham Pharmacia Biotech (Uppsala, Sweden). The fluorescent probe conjugation was performed with a maleimide derivative of AF 488 (Molecular Probes) with a C5 linker. All other chemicals were purchased from Sigma-Aldrich (St. Louis, MO) and used without further purification.

The C28W(1b) peptide from PMCA isoform 1b was synthesized by BioSource International (Hopkinton, MA). Its mass was checked by electrospray ionization mass spectrometry. T34C-CaM and T110C-CaM were expressed, purified, and fluorescently labeled following methods described previously (*22*). The preparation of T110C-CaM was conducted like that of T34C-CaM. Unlabeled T34C-CaM (used for competition experiments) was purified from *E. coli* cell paste with a phenyl-Sepharose column, eluted by addition of EDTA, and dialyzed twice with a large excess volume of buffer [HEPES (pH 7.4) and ~300 μM $CaCl_2$] to return CaM to its high-Ca^{2+} state.

Fluorescence Labeling and Oxidation. CaM was fluorescently labeled in the N-terminal domain at residue 34 or in the C-terminal domain at residue 110. The labeled proteins are denoted T34C-CaM-AF488 and T110C-CaM-AF488. For conjugation with AF488 C5 maleimide, T34C-CaM, or T110C-CaM was diluted to a final concentration of 50−100 μM. A 10-fold molar excess of TCEP was added to prevent intermolecular disulfide bond formation. AF488 C5 maleimide was dissolved in HEPES buffer and added dropwise to a final molar ratio of 12:1 (dye:protein). After the mixture had been stirred at room temperature for 1 h, the reaction was quenched by the addition of a 5:1 excess of glutathione to dye. The free dye was separated from the protein with the use of a Sephadex G-25 size-exclusion column followed by dialysis in 4 L of buffer [10 mM HEPES-NaOH (pH 7.4), 100 mM KCl, 1.0 mM $MgCl_2$, and 100 μM $CaCl_2$]. The labeling percentage was approximately 75%. No attempt was made to separate unlabeled protein, as it does not interfere with the kinetics of peptide release from labeled proteins. Control experiments in our laboratory have shown little or no effect of conjugation of a dye to CaM with regard to interaction with or activation of target enzymes (ref *22* and Supporting Information in ref *23*). For oxidation, CaM-AF488 was incubated with 10 mM H_2O_2 overnight at room temperature. Following oxidation, extensive dialysis was carried out to remove H_2O_2. Of the nine methionine residues, some are more solvent-exposed than others and are thus oxidized more readily (*17*). Using mass spectrometry, it was shown that the extent of oxidation was nearly uniform: the sample was a mixture of CaM species with seven, eight, or nine methionine residues oxidized (data not shown).

Sample Conditions. Final buffer conditions were as follows: 10 mM HEPES-NaOH (pH 7.4), 100 mM KCl, 1.0 mM $MgCl_2$, and 100 μM $CaCl_2$. The free Ca^{2+} concentration of the solutions was checked with the Ca^{2+} indicator dye Rhod-5n calibrated with respect to a calcium calibration kit (Molecular Probes, Eugene, OR). For competition experiments after addition of unlabeled CaM, the free Ca^{2+} concentration was 150 μM. For binding experiments, the free Ca^{2+} concentration was 105 μM.

Kinetic Studies. The fluorescence of AF488 was monitored at 517 nm with a Varian fluorimeter with excitation at 490 nm. Excitation slits were set at 1.5 nm, and emission

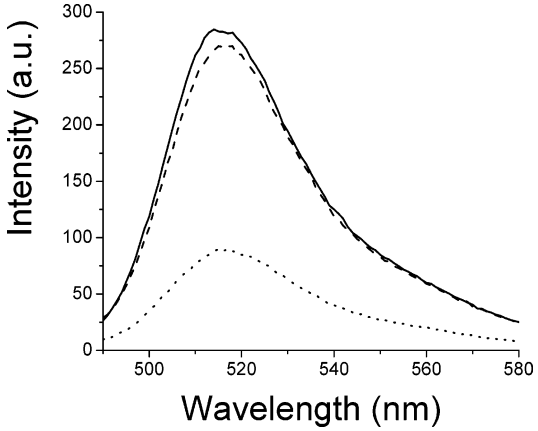

FIGURE 1: Fluorescence spectra of (—) T34C-CaM-AF488, (···) T34C-CaM-AF488 with C28W(1b) (2.0 μM), and (- - -) T34C-CaM-AF488 showing recovery 1.5 h after addition of excess, unlabeled CaM (see the text).

slits were set at 5 nm. For dissociation experiments, CaM-AF488 (70 nM) was incubated with C28W(1b) (3.0 μM) for up to 1 h. The fluorescence was monitored while adding a volume of 100 μL of concentrated unlabeled T34C-CaM to yield a final concentration of 25 μM unlabeled T34C-CaM for a >300-fold molar excess with respect to CaM-AF488. Upon dissociation of T34C-CaM-AF488 from C28W-(1b), there was a high probability that C28W(1b) would bind to the excess of T34C-CaM and not back to the minority species T34C-CaM-AF488. The fluorescence of T34C-CaM-AF488 was significantly higher in the absence of bound C28W(1b) (see Figure 1), and therefore, the overall fluorescence increased as C28W(1b) dissociated. The increase in fluorescence was monitored at 10 Hz. Fluorescence counts were binned before fitting to reduce noise. Control experiments consisting of the addition of 100 μL of buffer to the incubated CaM-AF488−C28W(1b) sample were carried out to estimate the mixing time under the stirring conditions. The mixing time was on the order of 0.5−1 s. The fluorescence output was recorded over the time scale of 100 ms to 10 000 s. No photobleaching was observed in control experiments for up to 1 h. The dissociation measurement was conducted for the N-terminal mutant, T34C-CaM-AF488, and the C-terminal mutant, T110C-CaM-AF488. Dissociation kinetic experiments were also carried out for T110C-CaM_{ox}-AF488 and T34C-CaM_{ox}-AF488. For binding studies, a small volume of concentrated C28W(1b) was added to T34C-CaM-AF488 (70 nM) in a stirred 3.0 mL cuvette. The final concentration of C28W(1b) was 3.0 μM.

Maximum Entropy Fitting. MemExp was used to fit all kinetic data (*24*). MemExp is a hybrid maximum-entropy, least-squares fitting program developed specifically for use in fitting complex kinetic data possessing information on multiple time scales (*25*). For fitting of the data, the uncertainty in fluorescence counts per period was assumed to be constant. Both increasing and decreasing contributions to the fluorescence change were allowed, but the data were best fit by maximum-entropy distributions with monotonic changes in fluorescence intensity, decreasing in the case of peptide binding or increasing in the case of dissociation of peptide from CaM. In each case, the fit recommended by MemExp was chosen as the best fit. This fit was the last iteration in which the goodness of fit parameter (χ^2) and the correlation length of the residuals both decreased by more than 1%.

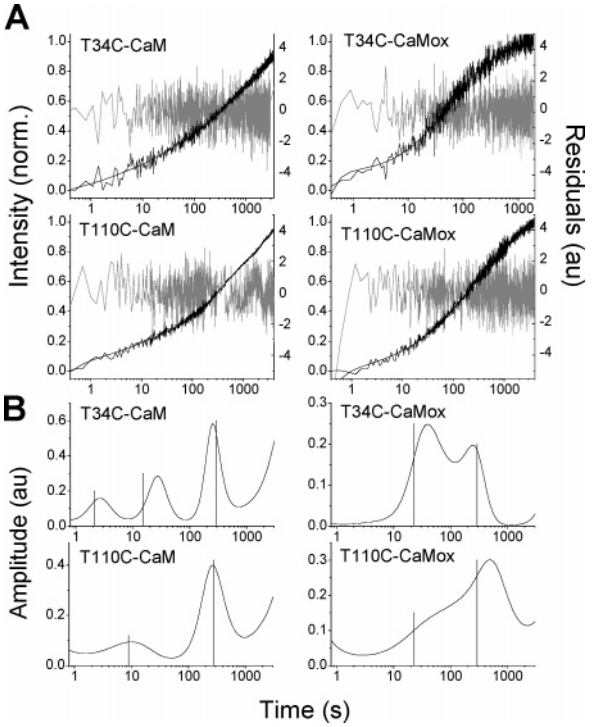

FIGURE 2: (A) Increase in the fluorescence of T34C-CaM-AF488, T110C-CaM-AF488, T34C-CaM_{ox}-AF488, and T110C-CaM_{ox}-AF488 upon dissociation from C28W(1b) plotted with a log time scale. Dissociation was detected by introduction of an excess of unlabeled T34C-CaM. The free Ca^{2+} concentration was 150 μM in each case. The MEM fits are shown as solid lines through the data, and the residuals are plotted in gray. (B) MEM fits for CaM dissociation for each of the four CaM-AF488 species. Lines are the inverse of the eigenvalues obtained after insertion of the rate constants from the best global fit back into the kinetic rate equations (see eqs S1 and S10).

RESULTS

The fluorescence of AF488 conjugated to CaM, at site 34 or 110, was quenched by 60−70% upon C28W(1b) binding. Examples of fluorescence spectra of 250 nM T34C-CaM-AF488 in the presence and absence of 2.0 μM C28W(1b) and after addition of excess unlabeled T34C-CaM are shown in Figure 1. The quenching was likely due to the proximity of the fluorescence label and the conserved tryptophan residue in C28W(1b). The results of kinetic measurements are shown in Figure 2. Upon dissociation of C28W(1b) from T34C-CaM-AF488 or T110C-CaM-AF488 in the presence of a large excess of unlabeled T34C-CaM, the fluorescence of the system increased. The free Ca^{2+} concentration for these solutions was 150 μM, as measured by the Ca^{2+} indicator dye Rhod-5n.

Maximum Entropy Fits. The time dependencies of the fluorescence increases in kinetic measurements consisted of multiple phases. In such cases, fitting the data to discrete exponentials requires an a priori assumption about the number of exponential components and is susceptible to the multiple-minimum problem (the fitted constants may depend on the initial guesses used in the fit). Such fits may not show conclusively whether an additional discrete time constant is justified, and the addition of an extra component may affect

Table 1: Time Constants of the MEM Fits to Kinetic Data, with Amplitudes in Parentheses

	time constant (s)		
Release Kinetics			
T34C-CaM-AF488	2.6 (18%)	26.5 (31%)	270 (51%)
T110C-CaM-AF488	8.4 (29%)		271 (71%)
T34C-CaM_{ox}-AF488	36 (64%)		238 (36%)
T110C-CaM_{ox}-AF488	118 (86%)		380 (14%)
Binding Kinetics			
T34C-CaM-AF488	3.2 (20%)		55 (80%)

the fitting parameters for other components. The maximum entropy method (MEM) is an excellent alternative for fitting complex data (*26*, *27*). MEM fits data to a distribution of rates to minimize χ^2 and simultaneously to maximize the smoothness of the fit (*28*). Additional peaks in the MEM distribution decrease the entropy (smoothness) and so appear only if the corresponding decrease in χ^2 is sufficient to offset the decrease in entropy. Thus, MEM does not require an a priori assumption of the number of kinetic constants and is useful in identifying the minimum number of rate constants required to fit the data.

The increases in fluorescence upon dissociation of T34C-CaM-AF488 and T110C-CaM-AF488 from C28W(1b) are shown in Figure 2, along with the MEM fits, the residuals, and the resulting MEM lifetime distributions. The data are plotted on a log time scale, with fluorescence counts normalized from 0 to 1 on the *y*-axis. The absence of a plateau at long times in the data is exaggerated by the logarithmic time scale and results from a longer phase in the fluorescence recovery (see below). The data and fits for dissociation of C28W(1b) from the oxidized species T34C-CaM_{ox}-AF488 and T110C-CaM_{ox}-AF488 are also shown in Figure 2. The peaks of the MEM lifetime distributions and their fractional amplitudes are listed in Table 1. Widths in the distributions are an unavoidable result of noise in the experimental data and may also reflect inhomogeneity in the kinetic processes.

MEM fits yielded three peaks for dissociation of T34C-CaM-AF488 and two peaks for dissociation of T110C-CaM-AF488 and for the two oxidized CaM species. Peak time constants and amplitudes are listed in Table 1. In all cases, an extremely long time constant on the order of several thousand seconds was also detected with an amplitude estimated to be less than 10% of the total recovery. Quantitative determination of the long time constant or amplitude was experimentally difficult due to photobleaching on this long time scale, even though steps were taken to minimize the influence of photobleaching, including minimizing exposure time and excitation intensity. As this step is more than 1 order of magnitude slower than the other processes, it can be excluded from the kinetic fit of the data with little effect on the modeling. It was therefore omitted to simplify the analysis. The extreme length of this time constant suggests that it is not relevant to the function of CaM. It may result from desorption of the protein from the glass walls of the cuvette.

Dissociation of C28W(1b) from T34C-CaM-AF488 showed the fastest peak (2.6 s). MemExp also predicted a fast distribution for T110C-CaM-AF488 centered at 8.4 s. Corresponding fast release processes were not found for dissociation of C28W(1b) from either of the oxidized species, with the fastest peak for T34C-CaM_{ox}-AF488 centered at 36 s. The best fit for T110C-CaM_{ox}-AF488 did not identify a well-resolved peak below 350 s, although there was a broad shoulder centered at 118 s. There were similarities in the MEM fits among the species that were important for modeling the data (see below). In all cases, a peak time constant was observed in the range of several hundred seconds (270 s for T34C-CaM-AF488, 271 s for T110C-CaM-AF488, 238 s for T34C-CaM_{ox}-AF488, and 380 s for T110C-CaM_{ox}-AF488; see Table 1). In addition, the predicted time constants were similar for T34C-CaM-AF488 and T34C-CaM_{ox}-AF488, except for the absence of a fast component in the case of T34C-CaM_{ox}-AF488. Oxidation also produced a decrease in the resolution of the peaks recovered from the MEM fits, especially for T110C-CaM-AF488, suggesting possible kinetic heterogeneity.

Table 2: Rate Constants (s^{-1}) Obtained from Modeling with eq 1[a]

	k_{-3}	k_3	k_{-2}	k_2	k_{-1}	k_{-c}
native CaM	0.0039	0.0088	0.14	0.20	0.21	0.11
	k_{-3}^{ox}	k_3^{ox}		k_{-c}^{ox}		
oxidized CaM	0.0039	0.0037		0.039		

[a] See the Supporting Information for further details.

To obtain more information for modeling kinetic steps involving the N-terminal domain, the binding of C28W(1b) to T34C-CaM-AF488 was also monitored and the resulting fluorescence decrease was fit by MEM (Figure 3). Two peaks were observed, corresponding to time constants of 3.2 and 54.7 s. The relative amplitudes for these peaks were 20 and 80%, respectively (Table 1). These data proved to be valuable for determining rate constants for intermediate steps in the binding pathway (see below).

Kinetic Modeling. The change in fluorescence intensity upon peptide release from fluorescently labeled CaM contains information about the mechanism of target binding and release (*29*). The MEM fit for the increase in fluorescence accompanying dissociation of C28W(1b) from T34C-CaM-AF488 had three peaks (excluding the longest component), suggesting a model with two intermediate species. One such model was proposed previously by Caride and co-workers for the kinetics of dissociation of CaM from the CaM-binding domain (C28W) of isoform 4b of PMCA (*14*, *15*) and is shown in Scheme 1, where B, I*, and UB represent "bound", "intermediate", and "unbound" species, respectively, and I_N is an intermediate possibly related to the release of the N-domain of CaM from C28W(1b) (see Discussion). Under the experimental conditions that were used (large molar excess of unlabeled T34C-CaM relative to T34C-CaM-AF488), the formation of UB can be considered irreversible due to trapping by the nonfluorescent CaM(wt)−C28W(1b) complex. The kinetic rate equations for this model can be solved by standard methods as described in the Supporting Information, yielding an expression for the predicted observable time constants in terms of the rates constants in Scheme 1 (eq S2 of the Supporting Information).

Upon addition of unlabeled T34C-CaM to the complex of C28W(1b) with T110C-CaM-AF488, the MEM fit indicated two kinetic processes and was best fit by MEM to two lifetime distributions centered at 8.4 and 271 s with relative amplitudes of 29 and 71%, respectively (Table 1 and

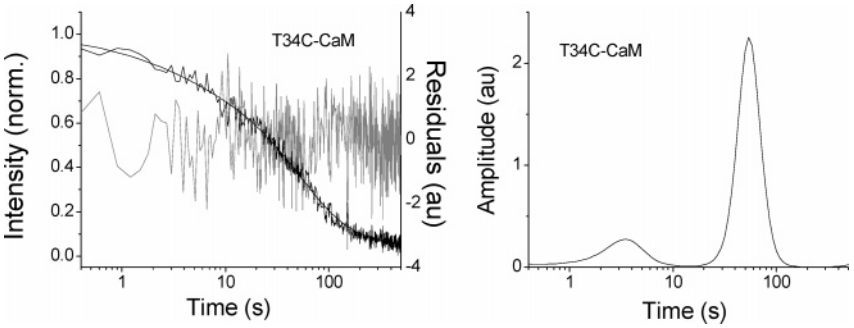

FIGURE 3: Decrease in the fluorescence of T34C-CaM-AF488 upon addition of C28W(1b) (left), along with the MEM fit (solid line through the data). The residuals are plotted in gray. The right panel shows the MEM distribution for binding of C28W(1b) to T34C-CaM-AF488.

Scheme 1

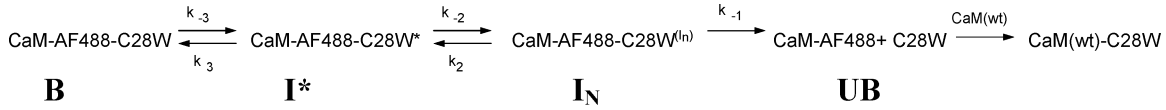

Scheme 2

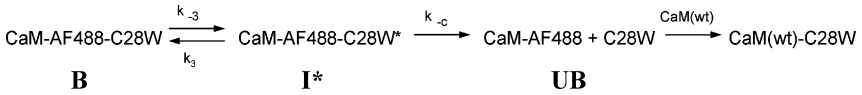

Figure 2). Therefore, these results can be described by a mechanism for dissociation that includes a single intermediate step. Such a mechanism is shown below in Scheme 2, which has been proposed previously by Török and Trentham for dissociation of peptides derived from smooth muscle myosin light chain kinase (*29*).

The kinetic rate equations for this model were solved by the same method used for Scheme 1, yielding expressions for the predicted observable rates (eq S11 of the Supporting Information).

We assumed that the predicted time constants for Scheme 1 or 2 correspond to the experimentally measured time constants that are represented by peaks in the MEM distributions. Therefore, we varied the values of the rate constants in Scheme 1 (k_3, k_{-3}, k_2, k_{-2}, and k_{-1}) or Scheme 2 (k_3, k_{-3}, k_{-c}, and k_{-1}) to obtain the best fit of the time constants predicted by the model to the observed MEM peaks. The determination of these rate constants allowed for calculation of the concentrations of the reactants, products, and intermediate species as a function of time (see eq S4 of the Supporting Information). As a function of time, the increase in fluorescence [$F(t)$] for both T34C-CaM-AF488 and T110C-CaM-AF488 is given by

$$F(t) = [\mathrm{B}](t)F_{\mathrm{B}} + [\mathrm{I}^*](t)F_{\mathrm{I}^*} + [\mathrm{I_N}](t)F_{\mathrm{IN}} + [\mathrm{UB}](t)F_{\mathrm{UB}} \quad (1)$$

where F_X is the relative fluorescence efficiency in state X.

In determining fits to the rate constants, we discuss first the determination of rate constants for Scheme 2. Then, results from fits to Scheme 2 are used as constraints to determine the rate constants for Scheme 1. If the longest component is excluded (thousands of seconds), it is convenient to fit the data for T110C-CaM-AF488 with the model proposed by Török and Trentham (*29*) (Scheme 2). With the rates and relative amplitudes (Table 1) obtained from the MEM fit for dissociation of C28W(1b) from T110C-CaM-AF488, rate constants k_{-3}, k_3, and k_{-c} were obtained (Table 2). The relative amplitudes obtained for the time constants from the MEM fit depend on the relative kinetic amplitudes from each kinetic step (or a combination of steps) scaled by the relative fluorescence intensities for each species (F_B, F_{I^*}, and F_{UB}). Initially, relative values of 1.0, 0.8, and 0.7 were chosen for F_{UB}, F_{I^*}, and F_B, respectively. The rate constants changed only slightly with changes in the values of F_{UB}, F_{I^*}, and F_B, provided that the fluorescence intensity of UB was higher than that of B, which must be true on the basis of the steady-state results (Figure 1).

The MEM fit for dissociation of C28W(1b) from T34C-CaM-AF488 showed three time constants (see Figure 2). Differences in MEM distributions for T34C-CaM-AF488 and T110C-CaM-AF488 were assumed to be due to differences in the sensitivity of the fluorescence intensity of the two domains to each of the kinetic steps. Thus, although Scheme 1 describes dissociation of C28W(1b) from both the N-terminally and C-terminally labeled mutants of CaM, the relative fluorescence yields of species B, I*, and I_N are not the same for T34C-CaM-AF488 and T110C-CaM-AF488. On the basis of the additional peak in the MEM distribution for T34C-CaM-AF488 relative to T110C-CaM-AF488, it is apparent that two of the T110C-CaM-AF488 species have similar fluorescence intensities so that their interconversion was not resolved. We therefore expected that the time constant of ca. 8 s reported by the MEM fit of T110C-CaM-AF488 corresponds to the steps with time constants of 2.6 and 26 s detected for T34C-CaM-AF488, and the individual steps are not resolved by the MEM fit for T110C-CaM-AF488 because the CaM labeled on the C-terminal domain is not sensitive to the formation of the I_N intermediate. Therefore, in the fit of the fluorescence data to eq 1, the $F_{I^*} = F_{In}$ constraint was set for T110C-CaM-AF488 but not necessarily for T34C-CaM-AF488. With this restriction, the amplitudes for each kinetic rate were varied along with the fluorescence intensity of each species to fit the fluorescence data (see eqs S7 and S9 of the Supporting Information).

Scheme 3

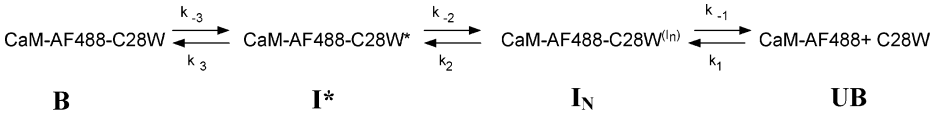

The equations obtained by solving the kinetic rate equations for Scheme 1 were insufficient to determine all of the rate constants, as there are five rate constants in Scheme 1 but only three equations (eq S2, for each non-zero eigenvalue ρ). Additional constraints were therefore necessary to fit the data. First, k_{-3} and k_3 were obtained from fits of the data for T110C-CaM-AF488 to Scheme 2 (see above). This is reasonable because the same slow time constant (~270 s) was obtained for both T34C-CaM-AF488 and T110C-CaM-AF488. Given these assumptions, multiple sets of values for k_{-2}, k_2, and k_{-1} still fit the experimental data. Further constraints on the values of the rate constants were therefore needed. These were obtained from the binding kinetics measured by the addition of concentrated C28W(1b) to T34C-CaM-AF488 shown in Figure 3.

For analysis of the binding experiment, it was necessary to include the binding step from UB to I_N. Scheme 1 was therefore modified to include k_1 (Scheme 3). The system of rate equations for Scheme 3 (see eq S13 of the Supporting Information) yielded further conditions for the kinetic rate constants. The fluorescence experiment reported here lacked the time resolution to directly measure k_1, which has been reported for various enzymes to be on the order of 10^8 M^{-1} s^{-1} (*14*, *15*, *30*). Caride and co-workers recently analyzed binding of CaM to the CaM-binding domain of isoform 4b of PMCA (*14*, *15*). It is widely believed that the initial encounter between CaM and its targets involves the C-terminal domain of CaM interacting with the N-terminal region of the target domain (*4*, *5*, *14*, *31*). The 18 N-terminal residues of C28W from isoforms 1b and 4b are identical. Therefore, we assumed that the rate constants for the initial encounter between CaM and these two isoforms are similar. The observed differences in the overall kinetics of association of CaM with the 1b and 4b isoforms of C28W are therefore likely due to differences in the contacts between CaM and the C-terminal regions of the C28W isoforms, which show some sequence variability (see below). Therefore, to model the data, we used the value for k_1 reported for binding of CaM to isoform 4b of C28W [4.6×10^8 M^{-1} s^{-1} (*14*)].

With k_3 and k_{-3} fixed as described above, the remaining rate constants were varied to find the best fit of the predicted rates in both Schemes 1 and 3 to the peaks found by MEM analysis. The rate constants that produced the best fit are listed in Table 2. From the best fit, the concentration of each species as a function of time is shown in Figure 4, and the relative fluorescence intensities of each species are listed in Table 3. As a check, the rate constants were substituted back into the kinetic rate equations (see eqs S2 and S11 of the Supporting Information), yielding time constants of 2.1, 15, and 291 s for T34C-CaM-AF488 in Scheme 1 (eq S2) and 8.8 and 276 s for T110C in Scheme 2 (eq S11). The values for T34C-CaM_{ox}-AF488 and T110C-CaM_{ox}-AF488 were 23 and 291 s, respectively. These values are shown as vertical lines in Figure 2. These time constants are consistent with the experimental dissociation time constants (Table 1). Sources of possible error include the use of a single time constant for a process that MEM fits with a distribution and the assumption that k_1 for isoform 4b (*14*) is the same as k_1 for isoform 1b (see Scheme 3).

Oxidized CaM. With only two experimental rate constants, an analysis based on Scheme 2 was sufficient for the fit of the dissociation data for oxidized CaM. The rates k_c, k_{-3}, and k_3 are here denoted k_{-c}^{ox}, k_{-3}^{ox}, and k_3^{ox}, respectively. The MEM distributions for T34C-CaM_{ox}-AF488 and T110C-CaM_{ox}-AF488 (Figure 2) did not exhibit a peak on the time scale of 1−20 s, suggesting that the fluorescence of AF488 at either domain is insensitive to any rapid interchange among intermediate species or that such interchange does not occur. Further, as opposed to the unoxidized species, for oxidized CaM the slow process (time scale of hundreds of seconds) is lower in amplitude than the faster process (time scale of tens of seconds for T34C-CaM_{ox}-AF488 or ~100 s for T110C-CaM_{ox}-AF488). For T110C-CaM_{ox}-AF488 and T34C-CaM_{ox}-AF488, the slower components had amplitudes of 14 and 36%, respectively. For the unoxidized species, the corresponding amplitudes were 71 and 51%, respectively (Table 1).

The experimental time constants for CaM_{ox} were fit following the methods used for T110C-CaM-AF488 to yield values for rate constants k_3^{ox}, k_{-3}^{ox}, and k_{-c}^{ox}. For the initial analysis, F_B^{ox} was set to 1.5 and F_{I*}^{ox} and F_{UB}^{ox} were set to 1.0. This analysis yielded values for k_{-3}^{ox} for both T110C-CaM_{ox}-AF488 and T34C-CaM_{ox}-AF488 that were similar to the value of k_{-3} for unoxidized CaM. This rate constant was therefore fixed to the value for unoxidized CaM. The same rate constants were used for T110C-CaM_{ox}-AF488 and T34C-CaM_{ox}-AF488, and differences in the MEM distributions were assumed to be due to differences in the relative fluorescence intensities of the intermediates for the N-terminally and C-terminally labeled proteins. With the amplitudes and experimental time constants from the MEM distributions, rate constants k_3^{ox} and k_{-c}^{ox} were varied along with the fluorescence intensities of F_B^{ox}, F_{I*}^{ox}, and F_{UB}^{ox} to generate a global fit to the dissociation data for both T110C-CaM_{ox}-AF488 and T34C-CaM_{ox}-AF488. The results of an iterative fit yielded the rate constants given in Table 2 and the relative fluorescence intensities of each species listed in Table 3. The value of k_3^{ox} for the final fit is lower for the oxidized proteins than the k_3 for unoxidized CaM as expected on the basis of the lower relative amplitude of the slower MEM peak for the oxidized proteins.

DISCUSSION

Binding Model. A number of studies have examined the kinetics of CaM binding and dissociation from targets such as myosin light chain kinase, CaM-dependent protein kinase II, and isoform 4b of PMCA (*14*, *15*, *29*−*33*). In each of these studies, a multiexponential time response was observed, suggesting mechanisms with at least one intermediate. To the best of our knowledge, this is the first study that systematically monitored dissociation kinetics with CaM

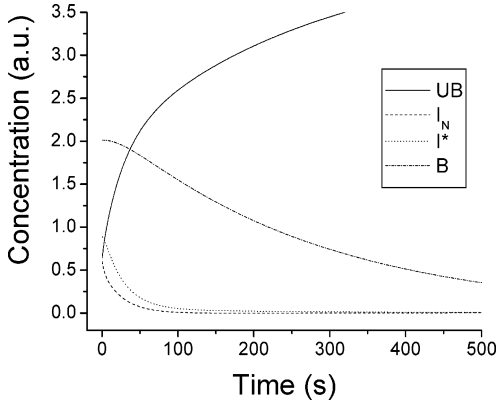

FIGURE 4: Modeled concentration of each species as a function of time for dissociation of C28W(1b) from CaM-AF488.

Table 3: Relative Fluorescence of Each Species from a Fit of the Data to eq 1[a]

	F(B)	*F*(I*)	*F*(I_N)	*F*(UB)
T34C-CaM-AF488	0.69	0.57	0.96	1.0
T110C-CaM-AF488	0.59	0.79	0.79	1.0
	F(B_{ox})	*F*(I^*_{ox})	*F*(UB_{ox})	
T34C-CaM_{ox}-AF488	0.65	0.68	1.0	
T110C-CaM_{ox}-AF488	0.72	0.93	1.0	

[a] For oxidized CaM, the fluorescence of each species was found from the iterative fit of T34C-CaM_{ox}-AF488 and T110C-CaM_{ox}-AF488 to eqs A11 and A12.

labeled on both the N-terminal and C-terminal domains. Perhaps the most interesting finding is the necessity for an additional time constant to fit the data for dissociation of C28W(1b) from T34C-CaM-AF488 relative to T110C-CaM-AF488. This result suggests, as has been proposed (*4*, *5*, *14*, *31*), that an intermediate step in the interaction of CaM with PMCA involves release of the N-terminal domain of CaM. T34C-CaM-AF488 would be expected to be sensitive to such a step, while T110C-CaM-AF488 may not be.

On the basis of the number of peaks in the MEM distributions, the model for dissociation of CaM from C28W(1b) must include two intermediate states. A similar model was employed previously for binding of CaM to C28W from isoform 4b of PMCA (*15*). Two of the intermediates must have similar fluorescence characteristics for CaM labeled on the C-terminal domain, because only one intermediate was detected for dissociation of T34C-CaM-AF647. A model that satisfies all of these conditions, shown in Figure 5, is based on Scheme 1 and on a model proposed previously for interaction of CaM with the binding domain of myosin light chain kinase (*34*). NMR results suggest that the formation of a tightly bound complex involves tight ionic contacts between the target helix and CaM (*34*, *35*). The model consists of a bound complex B between CaM and C28W(1b), where the domains of CaM interact tightly with a fully helical C28W(1b) peptide.

The first step in the dissociation pathway involves structural rearrangements from the compact, collapsed complex in which the C28W(1b) peptide is predominantly helical to a less compact and more open form (*34*, *35*). The C28W(1b) helix is destabilized, and partial unwinding of the helix occurs during this step. The I_N state is then formed as the

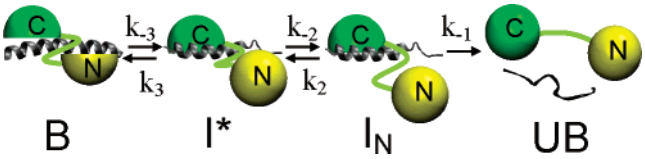

FIGURE 5: Model for dissociation of CaM from C28W(1b). B represents the bound CaM−C28W(1b) complex with a helical CaM-binding domain. In the intermediate I*, the C28W(1b)-binding domain is not fully helical. In I_N, the N-terminal domain of CaM is dissociated from the peptide. UB represents the fully unbound state.

C28W(1b) peptide unwinds to form a random coil structure and the N-terminal domain of CaM releases. Release of the C-terminal domain of CaM completes the dissociation process. The experiments presented here were conducted in the presence of 150 μM free Ca^{2+}, a concentration that is high enough to saturate Ca^{2+} binding in both domains of CaM. Therefore, it is unlikely that any of the observed intermediates in this study are caused by release of a Ca^{2+}-free N-terminal domain. Rather, it is likely that the ordered release of the N- and C-terminal domains occurs with two Ca^{2+} ions still bound in each domain.

Within the framework of this mechanism, the results in Table 3 reflect the structural changes that accompany rearrangement of compact complex B to intermediate I*. The distance between the tryptophan in C28W(1b) (Trp8, responsible for the fluorescence quenching in the complex) and the fluorescence probe is increased substantially upon conversion of B to I* when the probe is in the C-terminal domain, as indicated by the relatively large fluorescence increase. The side chain of this tryptophan residue is presumably bound in the hydrophobic cleft of the C-terminal domain of CaM (*4*). Therefore, upon conversion of B to I*, both orientational changes of the peptide in the C-terminal binding cleft and concomitant structural changes in the C-terminal domain promote a significant distance change between the C-terminal fluorescent probe and the tryptophan in the C28W(1b) peptide. Conversely, the distance between the tryptophan in C28W(1b) and the fluorescence probe is decreased when the probe is in the N-terminal domain (T34C-CaM-AF488), as demonstrated by the moderate decrease in fluorescence when B is converted to I*. This change is smaller than that observed when the probe is in the C-terminal domain and reflects a repositioning of the N-terminal domain relative to the tryptophan in the C28W(1b) peptide perhaps due to unwinding and bending of the C28W(1b) helix. Conversion to I_N is accompanied by a large change in the fluorescence of the complex when the probe is in the N-terminal domain, consistent with dissociation of the N-terminal domain of CaM from the peptide, but no fluorescence change when the probe is in the C-terminal domain, indicating little change in the interaction of the C-terminal domain and the C28W(1b) peptide.

Relationship of the Model to Previous Work. The model in Figure 5 is consistent with other models presented in the literature. Török and co-workers measured the binding and dissociation kinetics for CaM with peptides from the CaM-binding domains of myosin light chain kinase (*29*) and CaM-dependent protein kinase II (*33*), with CaM labeled in the central linker region or with a donor−acceptor pair. The kinetics could be modeled by a two-step mechanism with a

```
1a -  LRRGQILWFRGLNRIQTQMDVVNAFQSG
1b -  LRRGQILWFRGLNRIQTQIrVVnAFrSS
4b -  LRRGQILWFRGLNRIQTQIkVVkAFhSS
4a -  LRRGQILWFRGLNRIQTQIEVINKFQTG
2b -  LRRGQILWFRGLNRIQTQIRVVKAFRSS
3f -  LRRGQILWFRGLNRIQTQVCWDGKKMLR
```

FIGURE 6: Sequences of the CaM-binding domains for different isoforms of PMCA (*37*, *38*). The first 18 residues (underlined) are identical for all isoforms. Differences between isoforms 1b and 4b are shown with lowercase letters.

single intermediate state. Caride and co-workers (for PMCA isoform 4b) and Persechini and co-workers (for myosin light chain kinase) suggested a CaM peptide binding pathway in which the C-domain of CaM binds first and then the N-domain, followed by further collapse of CaM around the target to form the final complex (*14*, *31*). The model presented here is also consistent with one proposed by Wand and co-workers based on NMR data of CaM binding to the CaM-binding domain of smooth muscle myosin light chain kinase, which predicts a binding intermediate consisting of CaM complexed with a partially helical target CaM-binding domain and a fully bound complex with a helical target binding domain (*34*, *35*).

Relationship to Isoform 4b. There are four isoforms of PMCA, and changes of only a few residues in the CaM-binding domain of some isoforms can greatly affect the interaction between PMCA and CaM (*6*). Despite being the most common isoform, isoform 1 has been rarely studied due to difficulties in expression (*12*, *13*). A detailed expression protocol has been developed and published recently (*36*). The characterization of binding of CaM to the peptide representing the CaM-binding domain of this isoform may be a useful precursor to studies with the intact enzyme.

Recently, two studies have examined the kinetics of binding of CaM to isoform 4b of PMCA and the CaM-binding domain of this isoform (*14*, *15*). The results of those studies suggest a mechanism for binding of CaM to isoform 4b in which the C-terminal domain of CaM binds first, followed by binding of the N-terminal domain and subsequent collapse of CaM around the target. Thus, the results reported here are consistent with the kinetics of binding of CaM to C28W from isoform 4b of PMCA. However, the rates reported here for binding to isoform 1b are much slower than those reported for binding of CaM to C28W from isoform 4b.

The fact that amino acid sequence differences between the CaM binding regions of these two isoforms are limited to the C-terminal segment (see below) suggests that these C-terminal amino acids control the strengths of interaction with CaM. Sequences of the CaM-binding domains for different isoforms of PMCA are shown in Figure 6. The first 18 N-terminal residues of the CaM-binding domains of these isoforms are identical. However, differences in the 10 C-terminal residues of these isoforms are sufficient to dramatically alter their CaM binding affinities (*36*, *37*). For instance, a recent study reported dissociation constants of binding of CaM to C28W peptides from isoforms 3f and 2b that were nearly 2 orders of magnitude apart (*38*), and these differences must originate in the sequence differences in the C-terminal portions of the respective CaM binding regions. Thus, the differences in the kinetics reported for isoforms 1b and 4b must be due to the amino acid sequence differences (only three of them, shown in lowercase in Figure 6) in the 10 C-terminal residues of the CaM-binding domains of isoforms 1b and 4b.

Hydrophobic interactions are thought to be the dominant force in target recognition and binding by CaM (*1*, *16*). However, it is unlikely that the changes in hydrophobicity can account for the changes in binding kinetics between the peptides for isoforms 1b and 4b. All of the residues involved in these differences have similar hydrophobicities. [Kyte and Doolittle hydrophobicity parameters are −4.5, −3.9, −3.5, and −3.2 for arginine, lysine, asparagine, and histidine, respectively (*39*).] Charge−charge interactions may contribute to the differences observed for the two isoforms of PMCA. Isoform 1b has an asparagine at position 23 and an arginine at position 26. At neutral pH, the asparagine would be neutral while the arginine would have a positive charge. In isoform 4b, these charges are switched: the lysine at reside 23 would have a positive charge while the histidine at residue 26 would be neutral. Altered interactions between negatively charged CaM residues and positively charged residues in C28W(1b) may thus explain the differences between the affinity of CaM for isoform 1b observed here relative to that of CaM for isoform 4b. This notion is consistent with the idea that these electrostatic contributions are important for the specificity of interactions (*34*, *35*). It should also be noted that the helix propensity of asparagine is significantly lower than that of arginine, lysine, or histidine, and a decreased helicity in the peptide domain could contribute to decreased rates of association if the N-terminal domain of CaM interacts preferentially with a helical segment.

Relation to PMCA Activation. The C28W(1b) peptide, which consists of the CaM-binding domain of PMCA, is located in the autoinhibitory region of the enzyme. This domain of PMCA blocks activity of the enzyme in the absence of CaM (*40*) but is released or dissociated when CaM binds, thus activating the enzyme. The formation of a helix in the CaM-binding domain of PMCA is believed to be necessary for the release of the autoinhibitory domain. The C-terminal domain of CaM is thought to bind more tightly to target binding domains than the N-terminal domain, even when both domains are loaded with Ca^{2+} (*5*). Binding of both the C- and N-terminal domains of CaM to the CaM-binding domain is required for activation of the enzyme (*5*). The formation of fully bound complex B in C28W(1b) may thus be related to the induction of conformational changes in PMCA necessary for release of the autoinhibitory domain. Nevertheless, as demonstrated by Caride and co-workers (*14*), the kinetics of binding of CaM to PMCA are more complex than binding to C28W because of the participation of the rest of the enzyme and the possibility of CaM binding to both the closed and open conformations of the autoinhibitory domain.

Changes upon Oxidation. The oxidation of methionine residues has been shown to reduce the potency of CaM to maximally activate PMCA (*17*−*19*). Interestingly, this loss in activity is not due to a lack of binding of CaMox to PMCA, but rather to a reduced activity of PMCA−CaMox complexes (*19*, *41*). The reduced productivity of CaMox binding has been linked to a reduced tendency for CaMox to generate structural changes in the CaM-binding domain

of PMCA that are necessary to induce dissociation of the autoinhibitory domain from the catalytic region of the enzyme to relieve autoinhibition (*21*, *41*, *42*). A recent study of structural changes of binding of CaM_{ox} to C28W(1b) suggests that these functional changes result from a reduced helical propensity upon oxidation of Met144 and Met145 in the C-terminal helix of CaM (*21*).

In this study, we found that the kinetics of dissociation of C28W(1b) are perturbed by oxidation of the methionine residues in CaM in the following ways. First, the fast dissociation time observed with CaM (2−10 s) was not observed in CaM_{ox}. Second, the intermediate dissociation time constant (36−118 s) had a higher relative amplitude for CaM_{ox} than the corresponding time constants for unoxidized CaM. This result corresponds to a smaller fraction of tight binding orientations for oxidized CaM relative to unoxidized CaM. The resulting shift in the equilibrium away from a fully helical binding domain is consistent with the reduced tendency for release of the autoinhibitory domain in PMCA bound to CaM_{ox} (*42*). As a result, the net dissociation time for C28W(1b) is faster from that for CaMox from unoxidized CaM.

The dissociation kinetics for CaMox suggest that a mechanistic model based on Scheme 2 can be applied to the dissociation kinetics for both T34C-CaM_{ox}-AF488 and T110C-CaM_{ox}-AF488. The absence of a third time constant for T34C-CaM_{ox}-AF488 in contrast to T34C-CaM-AF488 suggests that the final step in the dissociation of C28W(1b) from CaM_{ox} does not result in different fluorescence signals when for the fluorescent probe is in the C- or N-terminal domain of CaM_{ox}. Thus, a distinct intermediate with one domain dissociated (I_N in Scheme 1) was not detected. This suggests either that dissociation of one domain is rapidly followed by dissociation of the other so that the $I_N \rightarrow$ UB step (Scheme 1) is not resolved, as suggested by the absence of a time constant of less than 10 s for CaMox, or that binding of the N- and C-terminal domains of CaMox may no longer be ordered and sequential, as it is for unoxidized CaM.

The rate constant k_3^{ox} for formation of the final complex (species B) of oxidized CaM and C28W(1b) is slower for oxidized CaM than it is for native CaM (Table 2), significantly altering the equilibrium for interconversion of B and I* relative to that of native CaM. The reduced rate of formation of species B with CaM_{ox} results in a predicted drop in the equilibrium constant for this step in Scheme 2 from 2.3 to 0.95. The resulting shift in the equilibrium away from a fully helical binding domain is consistent with the weakened tendency for release of the autoinhibitory domain in PMCA. The reduction of this rate may shift the equilibrium sufficiently to reduce the likelihood that oxidized CaM induces the necessary structural changes in the target that ultimately promote dissociation of the autoinhibitory domain. This result is consistent with the observation that for species B, the N- and C-terminal domains of CaM are closer in space in the CaM_{ox}−C28W(1b) complex than in the CaM−C28W-(1b) complex (*41*). As described above, we speculate that elongation of C28W(1b) as it becomes helical in the final binding step for unoxidized CaM is responsible for the increase in the fluorescence of T34C-CaM-AF488 for species B relative to I* (Table 3). A lack of full helix formation would preclude this result. As expected for oxidized CaM, the fluorescence yield of B was not increased relative to that of I* for T34C-CaM_{ox}-AF488 (Table 3), consistent with a final bound complex with oxidized CaM in which C28W-(1b) is not fully helical.

CONCLUSIONS

The fluorescence of AF488 conjugated to CaM is sensitive to the binding and dissociation of C28W(1b), the CaM-binding domain of PMCA. Two CaM mutants, one with AF488 conjugated to residue 34 in the N-domain and the other to residue 110 in the C-domain, were used to elucidate the nature of different species in the dissociation pathway. The results indicate that binding of C28W(1b) involves an intermediate consisting of a bound C-domain with a free N-domain, followed by N-domain binding with partial helix formation of the target, and finally a slight increase in the distance between lobes of CaM as the helix fully forms. Previous measurements with CaM labeled at Lys75 (*15*) also favored a model in which CaM binds to C28W from isoform 4b of PMCA in three reversible steps with two intermediates. These results for isoform 1b are consistent with that kinetic model but with rates constants that are lower by at least 1 order of magnitude. Furthermore, by using CaM with fluorescence labels in either the N- or C-terminal domains, these results also reveal the different roles of the N- and C-terminal domains in the individual kinetic steps. Analysis of the dissociation kinetics for oxidized CaM suggests that CaM_{ox} is less likely to form a tight binding complex due to a decrease in the rate of formation of this complex. These results support the idea that induction of helical structure in the CaM-binding domain of PMCA is an obligatory step for relief of autoinhibition and enzyme activation.

ACKNOWLEDGMENT

We thank Professor Richard Schowen for insightful discussions regarding binding kinetics.

SUPPORTING INFORMATION AVAILABLE

Kinetic rate equations and solutions required for analysis of the kinetic data. This material is available free of charge via the Internet at http://pubs.acs.org.

REFERENCES

1. Vetter, S. W., and Leclerc, E. (2003) Novel Aspects of Calmodulin Target Recognition and Activation, *Eur. J. Biochem. 270*, 404−414.
2. Bayley, P., Ahlstrom, P., Martin, S. R., and Forsen, S. (1984) The Kinetics of Calcium Binding to Calmodulin: Quin 2 and ANS Stopped-Flow Fluorescence Studies, *Biochem. Biophys. Res. Commun. 120*, 185−191.
3. VanScyoc, W. S., Sorensen, B. R., Rusinova, E., Laws, W. R., Ross, J. B. A., and Shea, M. A. (2002) Calcium Binding to Calmodulin Mutants Monitored by Domain-Specific Intrinsic Phenylalanine and Tyrosine Fluorescence, *Biophys. J. 83*, 2767−2780.
4. Elshorst, B., Hennig, M., Foersterling, H., Diener, A., Maurer, M., Schulte, P., Schwalbe, H., Griesinger, C., Krebs, J., Schmid, H., Vorherr, T., and Carafoli, E. (1999) NMR Solution Structure of a Complex of Calmodulin with a Binding Peptide of the Calcium Pump, *Biochemistry 38*, 12320−12332.
5. Sun, H., and Squier, T. C. (2000) Ordered and Cooperative Binding of Opposing Globular Domains of Calmodulin to the Plasma Membrane Ca-ATPase, *J. Biol. Chem. 275*, 1731−1738.
6. Penniston, J. T., and Enyedi, A. (1998) Modulation of the Plasma Membrane Ca^{2+} Pump, *J. Membr. Biol. 165*, 101−109.

7. Carafoli, E., and Brini, M. (2000) Calcium Pumps: Structural Basis for and Mechanism of Calcium Transmembrane Transport, *Curr. Opin. Chem. Biol. 4*, 152−161.
8. Gao, J., Yin, D. H., Yao, Y., Sun, H., Qin, Z., Schöneich, C., Williams, T. D., and Squier, T. C. (1998) Loss of Conformational Stability in Calmodulin Upon Methionine Oxidation, *Biophys. J. 74*, 1115−1134.
9. Kataoka, M., Head, J. F., Vorherr, T., Krebs, J., and Carafoli, E. (1991) Small-Angle X-ray Scattering Study of Calmodulin Bound to Two Peptides Corresponding to Parts of the Calmodulin-Binding Domain of the Plasma Membrane Ca^{2+} Pump, *Biochemistry 30*, 6247−6251.
10. Chapman, E. R., Alexander, K., Vorherr, T., Carafoli, E., and Storm, D. R. (1992) Fluorecence Energy Transfer Analysis of Calmodulin-Peptide Complexes, *Biochemistry 31*, 12819−12825.
11. Stauffer, T. P., Hilfiker, H., Carafoli, E., and Strehler, E. E. (1993) Quantitative Analysis of Alternative Splicing Options of Human Plasma Membrane Calcium Pump Genes, *J. Biol. Chem. 268*, 25993−26003.
12. Adamo, H. P., Verma, A. K., Sanders, M. A., Heim, R., Salisbury, J. L., Wieben, E. D., and Penniston, J. T. (1992) Overexpression of the Erythrocyte Plasma Membrane Ca^{2+} Pump in Cos-1 Cells, *Biochem. J. 285*, 791−797.
13. Liu, B. F., Xu, X., Fridman, R., Muallem, S., and Kuo, T. H. (1996) Consequences of Functional Expression of the Plasma Membrane Ca^{2+} Pump Isoform 1a, *J. Biol. Chem. 271*, 5536−5544.
14. Penheiter, A. R., Bajzer, Z., Filoteo, A. G., Thorogate, R., Török, K., and Caride, A. J. (2003) A Model for the Activation of Plasma Membrane Calcium Pump Isoform 4b by Calmodulin, *Biochemistry 42*, 12115−12124.
15. Penheiter, A. R., Filoteo, A. G., Penniston, J. T., and Caride, A. J. (2005) Kinetic Analysis of the Calmodulin-Binding Region of the Plasma Membrane Calcium Pump Isoform 4b, *Biochemistry 44*, 2009−2020.
16. Crivici, A., and Ikura, M. (1995) Molecular and Structural Basis of Target Recognition by Calmodulin, *Annu. Rev. Biophys. Biomol. Struct. 24*, 85−116.
17. Yao, Y., Yin, D., Jas, G. S., Kuczera, K., Williams, T. D., Schöneich, C., and Squier, T. C. (1996) Oxidative Modification of a Carboxyl-Terminal Methionine in Calmodulin by Hydrogen Peroxide Inhibits Calmodulin-Dependent Activation of the Plasma Membrane Ca-ATPase, *Biochemistry 35*, 2767−2787.
18. Gao, J., Yao, Y., Williams, T. D., and Squier, T. C. (1998) Progressive Decline in the Ability of Calmodulin Isolated from Aged Brain to Activate the Plasma Membrane Ca-ATPase, *Biochemistry 37*, 9536−9548.
19. Bartlett, R. K., Bieber Urbauer, R. J., Anbanandam, A., Smallwood, H. S., Urbauer, J. L., and Squier, T. C. (2003) Oxidation of Met144 and Met145 in Calmodulin Blocks Calmodulin Dependent Activation of the Plasma Membrane Ca-ATPase, *Biochemistry 42*, 3231−3238.
20. Squier, T. C., and Bigelow, D. J. (2000) Protein Oxidation and Age-Dependent Alterations in Calcium Homeostasis, *Front. Biosci. 5*, 504−526.
21. Anbanandam, A., Bieber Urbauer, R. J., Bartlett, R. K., Smallwood, H. S., Squier, T. C., and Urbauer, J. L. (2005) Mediating Molecular Recognition by Methionine Oxidation: Conformational Switching by Oxidation of Methionine in the Carboxyl-Terminal Domain of Calmodulin, *Biochemistry 44*, 9486−9496.
22. Allen, M. W., Urbauer, R. J. B., Zaidi, A., Williams, T. D., Urbauer, J. L., and Johnson, C. K. (2004) Fluorescence Labeling, Purification and Immobilization of a Double Cysteine Mutant Calmodulin Fusion Protein for Single-Molecule Experiments, *Anal. Biochem. 325*, 273−284.
23. Slaughter, B. D., Unruh, J. R., Price, E. S., Huynh, J. L., Bieber Urbauer, R. J., and Johnson, C. K. (2005) Sampling Unfolding Intermediates in Calmodulin by Single-Molecule Spectroscopy, *J. Am. Chem. Soc. 127*, 12107−12114.
24. Steinbach, P. J., Ionescu, R., and Matthews, C. R. (2002) Analysis of Kinetics Using a Hybrid Maximum-Entropy/Nonlinear-Least-Squares Method: Application to Protein Folding, *Biophys. J. 82*, 2244−2255.
25. Cornwell, T. J., and Evans, K. F. (1985) A Simple Maximum Entropy Deconvolution Algorithm, *Astron. Astrophys. 143*, 77−83.
26. Swaminathan, R., and Periasamy, N. (1996) Analysis of Fluorescence Decay by the Maximum Entropy Method: Influence of Noise and Analysis Parameters on the Width of the Distribution of Lifetimes, *Proc. Indian Acad. Sci. Chem. Sci. 108*, 39−49.
27. Steinbach, P. J. (1996) Two-Dimensional Distributions of Activation Enthalpy and Entropy from Kinetics by the Maximum Entropy Method, *Biophys. J. 70*, 1521−1528.
28. Brochon, J. C. (1994) Maximum Entropy Method of Data Analysis in Time-Resolved Spectroscopy, *Methods Enzymol. 240*, 262−311.
29. Török, K., and Trentham, D. R. (1994) Mechanism of 2-Chloro-(ϵ-amino-Lys_{75})-[6-[4-(*N*,*N*-diethylamino)phenyl]-1,3,5-triazin-4-yl]calmodulin Interactions with Smooth Muscle Myosin Light Chain Kinase and Derived Peptides, *Biochemistry 33*, 12807−12820.
30. Török, K., Cowley, D. J., Brandmeier, B. D., Howell, S., Aitken, A., and Trentham, D. R. (1998) Inhibition of Calmodulin-Activated Smooth-Muscle Myosin Light-Chain Kinase by Calmodulin-Binding Peptides and Fluorescent (Phosphodiesterase-Activating) Calmodulin Derivatives, *Biochemistry 37*, 6188−6198.
31. Persechini, A., McMillan, K., and Leakey, P. (1994) Activation of Myosin Light Chain Kinase and Nitric Oxide Synthase Activities by Calmodulin Fragments, *J. Biol. Chem. 269*, 16148−16154.
32. Brown, S. E., Martin, S. R., and Bayley, P. M. (1997) Kinetic Control of the Dissociation Pathway of Calmodulin-Peptide Complexes, *J. Biol. Chem. 272*, 3389−3397.
33. Török, K., Tzortzopoulos, A., Grabarek, Z., Best, S. L., and Thorogate, R. (2001) Dual Effect of ATP in the Activation Mechanism of Brain Ca^{2+} Calmodulin-Dependent Protein Kinase II by Ca^{2+} Calmodulin, *Biochemistry 40*, 14878−14890.
34. Ehrhardt, M. R., Urbauer, J. L., and Wand, A. J. (1995) The Energetics and Dynamics of Molecular Recognition by Calmodulin, *Biochemistry 34*, 2731−2738.
35. Kranz, J. K., Flynn, P. F., Fuentes, E. J., and Wand, A. J. (2002) Dissection of the Pathway of Molecular Recognition by Calmodulin, *Biochemistry 41*, 2599−2608.
36. Brini, M., Coletto, L., Pierobon, N., Kraev, N., Guerini, D., and Carafoli, E. (2003) A Comparative Functional Analysis of Plasma Membrane Ca^{2+} Pump Isoforms in Intact Cells, *J. Biol. Chem. 278*, 24500−24508.
37. Enyedi, A., Filoteo, A. G., Gardos, G., and Penniston, J. T. (1991) Calmodulin-Binding Domains from Isozymes of the Plasma Membrane Ca^{2+} Pump Have Different Regulatory Properties, *J. Biol. Chem. 266*, 8952−8956.
38. Filoteo, A. G., Enyedi, A., Verma, A. K., Elwess, N. L., and Penniston, J. T. (2000) Plasma Membrane Ca^{2+} Pump Isoform 3f Is Weakly Stimulated by Calmodulin, *J. Biol. Chem. 275*, 4323−4328.
39. Kyte, J., and Doolittle, R. F. (1982) A Simple Method for Displaying the Hydropathic Character of a Protein, *J. Mol. Biol. 157*, 105−132.
40. Enyedi, A., Vorherr, T., James, P., McCormick, D. J., Filoteo, A. G., Carafoli, E., and Penniston, J. T. (1989) The Calmodulin Binding Domain of the Plasma Membrane Ca^{2+} Pump Interacts Both with Calmodulin and with Another Part of the Pump, *J. Biol. Chem. 264*, 12313−12321.
41. Gao, J., Yao, Y., and Squier, T. C. (2001) Oxidatively Modified Calmodulin Binds to the Plasma Membrane Ca-ATPase in a Nonproductive and Conformationally Disordered Complex, *Biophys. J. 80*, 1791−1801.
42. Osborn, K. D., Bartlett, R. K., Mandal, A., Zaidi, A., Urbauer, R. J. B., Urbauer, J. L., Galeva, N., Williams, T. D., and Johnson, C. K. (2004) Single-Molecule Dynamics Reveal an Altered Conformation for the Autoinhibitory Domain of Plasma-Membrane Ca^{2+}-ATPase Bound to Oxidatively Modified Calmodulin, *Biochemistry 43*, 12937−12944.

BI602481U